SURFACE AND INTERFACE ANALYSIS, VOL. 24, 363–370 (1996)

Surface Analysis by SNMS: Femtosecond Laser Postionization of Sputtered and Laser Desorbed Atoms

Günther K. Nicolussi,[1,4,*] Michael J. Pellin,[1] Keith R. Lykke,[1] Jennifer L. Trevor,[1,2] Donald E. Mencer[3] and Andrew M. Davis[4]

[1] Materials Science and Chemistry Divisions, Argonne National Laboratory, Argonne, IL 60439, USA
[2] Department of Chemistry, University of Illinois at Chicago, Chicago, IL 60607, USA
[3] Department of Chemistry, Aurora University, Aurora, IL 60506, USA
[4] Enrico Fermi Institute, University of Chicago, Chicago, IL 60637, USA

The photoionization efficiency of secondary neutral atoms from metal surfaces has been investigated by very intense ($\sim 10^{14}$ W cm^{-2}) and short-pulsed ($\sim$200 fs) 248 nm laser radiation. Surface erosion of the samples was performed by Ar^+ ion sputtering and by laser desorption (LD) from an N_2 gas laser. Five polycrystalline samples (Al, Cu, Zr, In and Au) have been analyzed with respect to their ionization efficiency and LD yields. In order to estimate the desorption yield, we determined the useful yield of our time-of-flight (ToF) mass spectrometer by ion sputtering, followed by laser postionization with 193 nm radiation from an ArF excimer laser. The applied femtosecond pulse, high-intensity 248 nm laser radiation has been found to be an excellent source of non-selective photoionization. For each material in this study a large fraction of doubly ionized atoms was observed; the measurements on Au have also shown triply ionized atoms. For some spectra, the number of doubly ionized atoms was even higher than for singly ionized atoms. We have estimated that the useful yields for LD are significantly higher than the values observed in ion sputtering.

INTRODUCTION

Sputtering by energetic ions has been used for decades for surface modification and analysis.[1] Surface composition can be determined by measuring either directly emitted secondary ions (secondary ion mass spectrometry, SIMS) or postionized secondary neutrals (secondary neutral mass spectrometry, SNMS). Due to the relatively low secondary ion yield for many materials and the large matrix effects, the postionization of secondary neutrals has become more and more important for surface analysis. In particular, ionization by resonant or non-resonant laser radiation has many advantages compared to other ionization techniques, such as electron impact[2] or RF plasma.[3] Resonant ionization of secondary atoms permits high selectivity as well as high efficiency; thus, it can be considered an ideal tool for trace analysis of a specific element.[4]

One advantage of intense, non-resonant laser radiation is the capability of ionizing different species simultaneously.[5] Laser radiation in the UV regime permits non-resonant, two-photon ionization for a large number of elements. For laser intensities above 10^{10} W cm^{-2}, saturation (100% ionization) is usually achieved.[6] Postionization of sputtered atoms and molecules has also been performed successfully with ultrahigh-intensity picosecond and femtosecond lasers using wavelengths in the visible and near-infrared regime.[7–9] The probability of non-resonant multiphoton ionization (NRMPI) scales with approximately I^n, where I is the laser intensity and n is the order of the process (the number of absorbed photons). It is obvious that high-order processes require much higher laser intensities for efficient NRMPI.

In the past few years, ion sputtering in combination with laser postionization has been widely used for analytical purposes and also for the investigation of basic processes in sputtering.[10–12] In a similar way, postionization of laser-desorbed atoms can be utilized to learn more about desorption processes.[13]

The advantage of ion sputtering relative to laser desorption (LD) is clearly the attainment of a constant fraction of sputtered atoms to incoming primary ions for a defined bombardment energy. This sputter yield is constant over a wide range of primary ion intensities as long as individual collision cascades do not interfere.[14] By knowing the sputter yield, the amount of material removed from the sample can be determined easily by measuring the target current. Unfortunately, this concept breaks down when more complex materials need to be analyzed. In addition, ions are subject to space-charge effects, so that an upper limit to the amount of removable material is readily achieved.

Laser microprobe mass spectrometry can be performed with directly emitted ions (analogous to SIMS), or it can be conjoined with postionization techniques of secondary neutrals.[15,16] The short-pulse nature of an ablation laser is well suited for time-of-flight mass spec-

* Author to whom correspondence should be addressed at: Argonne National Laboratory, Materials Science and Chemistry Divisions, 9700 S. Cass Avenue, Bldg. 200, Argonne, IL 60439, USA.

CCC 0142-2421/96/060363–08

Received 4 December 1995
Accepted 22 February 1996

trometry (ToF-MS), since laser pulses of the order of nanoseconds are negligible on the time scale of ToF-MS. Secondary particle yields from solid metal targets will depend strongly on the incident energy density and the affected volume of the solid. Energy deposition into the solid is a non-equilibrium thermal process. The relevant variables for the incident energy density are laser intensity at the surface, sample reflectivity, optical absorptivity, thermal conductivity, melting temperature, heat capacity and latent heat of vaporization.[17] For high laser intensities (typically $<10^{10}$ W cm^{-2}), a dense plasma is formed above the target surface. In this mode of operation, particle emission occurs in the initial phase of the laser pulse. A substantial part of the laser radiation interacts with this particle cloud and increases temperatures, ion density and electron density. As a consequence, laser microprobe analysis under plasma conditions is not favorable for the analysis of molecules due to their sensitivity towards fragmentation. Furthermore, the mass resolution is usually low, due to space–charge-induced acceleration of secondary ions.[18]

At lower intensities a 'soft' removal of atoms and molecules from surfaces is possible by laser-induced thermal desorption. Large, non-volatile and often fragile molecules can be introduced into a mass spectrometer intact and very efficiently by LD from a substrate, whereas ion-stimulated desorption results in substantial fragmentation.[19] The spatial resolution of laser-desorbed particles can be in the submicron regime and is virtually limited only by the focal characteristics of the laser beam.

In this work, we will characterize LD with high spatial resolution for postionized atoms. Moreover, the relevant parameters for an efficient laser postionization of laser-desorbed particles will be investigated. In particular, we will discuss NRMPI by very intense femtosecond laser radiation.

EXPERIMENTAL

The present studies have been performed on a new type of apparatus that has been described in detail in a recent paper.[20] The Chicago Argonne Resonant Ionization Spectrometer for MicroAnalysis (CHARISMA) apparatus has been developed as part of a collaboration between Argonne National Laboratory and the University of Chicago. A schematic diagram of the apparatus is shown in Fig. 1. The instrument, located at Argonne, is composed of a primary ion gun, the main chamber with an XYZ rotational target stage, a reflectron-type ToF mass spectrometer and the optical arrangement for laser ablation and laser postionization. The instrument design incorporates modes for both conventional ion beam analysis and laser microanalysis. The experiments have been performed on poly-

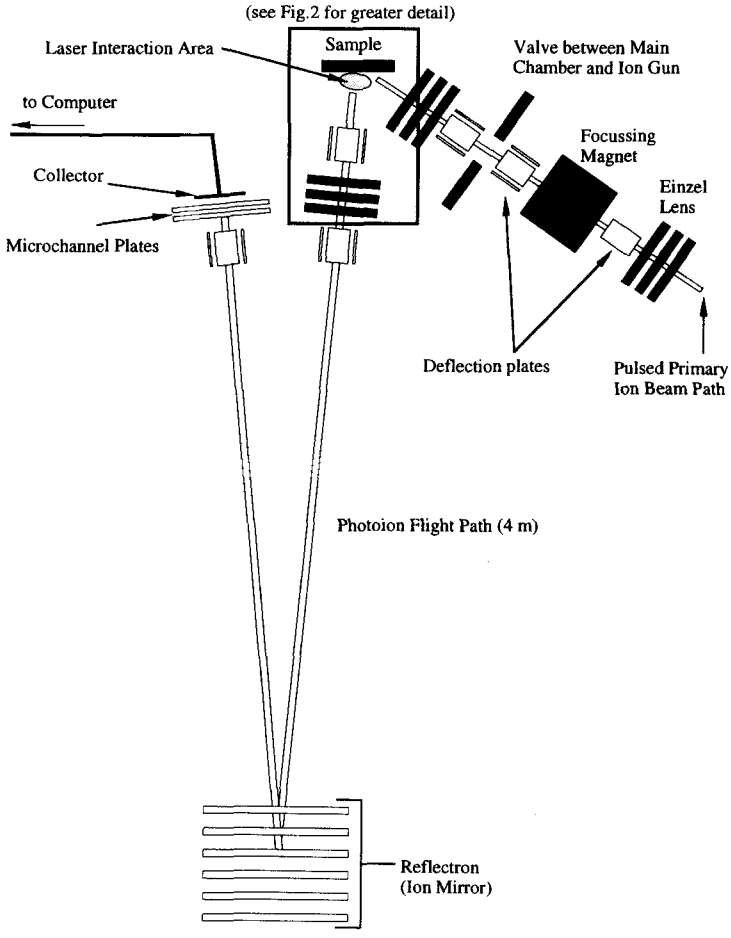

Figure 1. Schematic diagram of the apparatus. The region around the sample and laser interaction area is expanded in Fig. 2.

crystalline samples of Al, Cu, Zr, In and Au. All samples had a diameter of 1 mm and were mounted on a stainless-steel holder. The XYZ motion of the target is attained by three high-precision in-vacuum piezoelectric inchworm motors (Burleigh) with a mechanical resolution of ~0.01 μm.

Ion sputtering of samples is accomplished with a 5 keV Ar^+ ion beam generated in a Colutron ion source. The primary ions strike the sample at an angle of 60° from the surface normal and with target currents as high as 2 μA. The diameter of the ion beam is ~0.5 mm. The ion sputtering experiments are usually performed in a pulsed mode with 800 ns Ar^+ ion pulses, which corresponds to $\sim 10^7$ primary ions per shot.

For laser microprobe analysis, the ablation laser is introduced onto the sample surface by means of a Schwarzschild microscope.[21] The two concentric and spherical mirrors of the microscope (see Fig. 2) ensure complete achromatism (reflective optics). Because of the all-reflecting nature of the Al mirrors (with MgF_2 coating), the Schwarzschild optics are able to introduce white light for sample viewing and the desorption laser light at the same time. The numerical aperture (NA) of our microscope is ~0.5, the magnification factor is 19 and the optical resolution is below 1 μm. It has been demonstrated that in this special Schwarzschild arrangement, the third-order aberrations (spherical, astigmatic and coma) of both mirrors cancel almost totally.[22]

For laser ablation, an N_2 gas laser with a wavelength of 337 nm and a pulse length of ~3 ns was used. By means of the Schwarzschild microscope, the laser beam was focused on the sample surface to a diameter of ~1 μm. The output of the N_2 laser was $\sim 10^{-4}$ J per pulse; however, the beam was attenuated for all LD experiments, and we estimate that the incident energy on the sample surfaces was < 100 nJ per pulse.

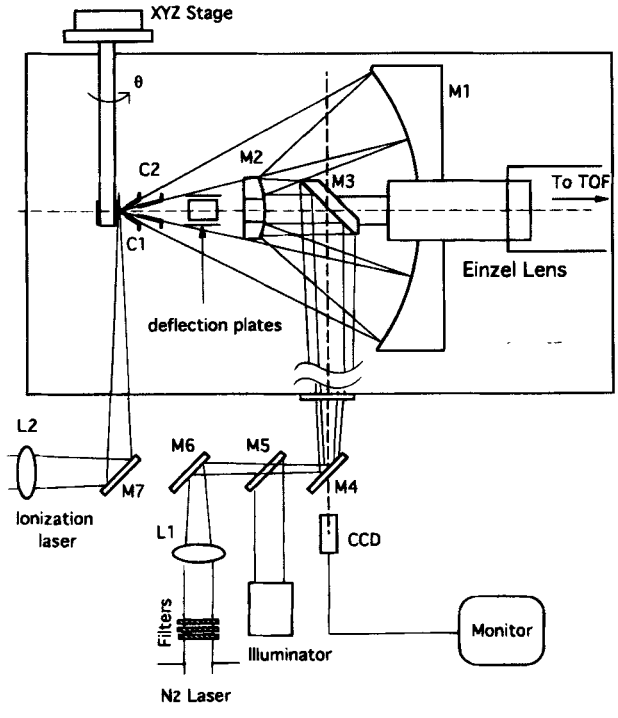

Figure 2. Schwarzschild microscope and optical arrangement: M = mirror, L = lens and C = conical extraction electrode. One of the filters in the N_2 laser beam is a circular, variable, neutral-density filter that allows continuous precise control of the laser energy.

The ToF mass spectrometer can simultaneously detect secondary ions and postionized secondary neutrals. The field-free drift tube of the spectrometer is at ground potential, with acceleration and extraction of the direct ions (or photoions) being achieved by pulsing the potential of the target and the extraction cone of the spectrometer. A well-controlled timing sequence of the primary ion pulse (or desorption laser pulse), the target pulse (+2000 V), the extraction pulse (+1800 V) and the postionizing laser pulse is essential to achieve a high useful yield in the mass spectrometer. Furthermore, an overlap of the direct ion signal and the photoion signal can only be established for a particular timing sequence.

Postionization of the ion-sputtered or laser-desorbed secondary neutrals was performed either by ArF excimer laser radiation (193 nm, pulse length ~20 ns) or femtosecond laser radiation (248 nm, pulse length 200 fs). Although the postionizing laser radiation can be introduced either parallel to the sample surface or perpendicular to the surface via the Schwarzschild microscope, in this work the 'traditional' parallel configuration has been used.

In the measurements performed with ArF laser ionization, the beam was intentionally defocused above the target surface to enlarge the ionization volume. The laser cross-section was ~4 mm^2 in front of the sample surface, and the average laser intensity in the ionization volume is $\sim 10^7$ W cm^{-2}. This combination of a large ionization volume at the expense of laser intensity is favorable for Al and In due to a one-photon process with high-ionization cross-sections. In contrast, for Cu, Zr and Au, a far less efficient two-photon process is required; hence, much lower signal levels can be expected.

The high-power, high-repetition-rate UV femtosecond system utilizes a homemade Ti:sapphire oscillator/regenerative amplifier and amplification of frequency-tripled light in a KrF excimer laser cavity. The laser is based on chirped-pulse amplification. Figure 3 shows the principal configuration of our femtosecond laser system. The Ti:sapphire oscillator[23] is pumped by an Ar ion laser and is capable of producing 15 fs pulses at 90 MHz and ~800 mW of power. For the present experiments, the femtosecond oscillator is tuned to ~746 nm (~20 nm width) with a pulse length of ~60 fs (measured with an autocorrelator). The pulses are then stretched to ~100 ps in an all-reflective grating stretcher. They are then amplified to ~0.8 mJ per pulse in a Ti:sapphire regenerative amplifier[24] (pumped by a frequency-doubled Nd:YAG laser). These pulses are then recompressed to ~100 fs in a two-grating compressor. This system now produces ~ 100 fs pulses with ~300 μJ pulse at 2 kHz. We then frequency double (in *LBO*, 1.5 mm crystal) and triple (in *BBO*, 0.5 mm crystal) the compressed output by mixing the fundamental with its second harmonic after rotating the plane of polarization of the fundamental beam and suitably delaying the red pulse relative to the blue pulse.[25]

The UV (248 nm) femtosecond pulses are ~1–5 μJ pulse with < 200 fs pulsewidth (measured by the autocorrelation of the fundamental with its second

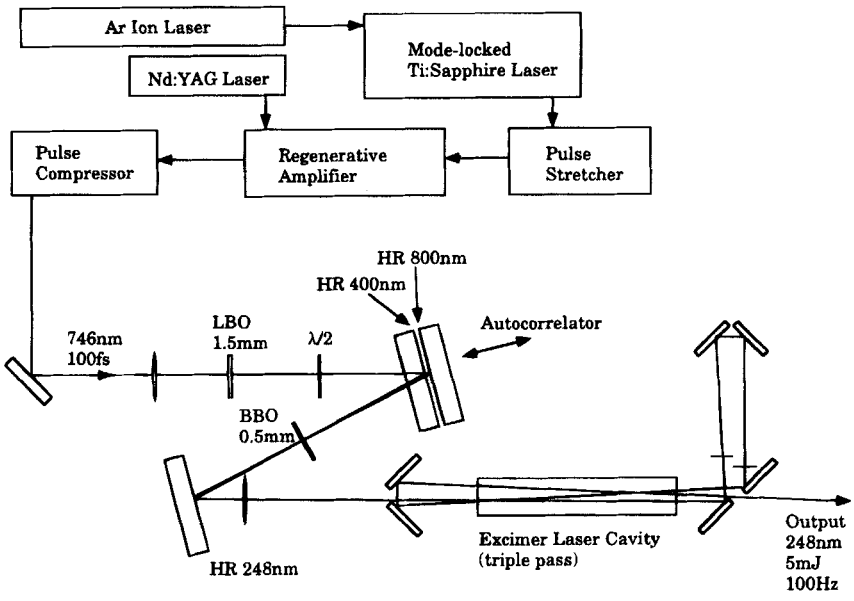

Figure 3. Schematic diagram of the femtosecond laser system.

harmonic). We then amplify this tripled light by triple-passing an excimer (Questek) laser amplifier.[26,27] The relative timing is critical and is matched by using photodiodes and a digital delay generator. The amplified output yields ~2–10 mJ of 248 nm femtosecond pulses at repetition rates of 100 Hz.

The 248 nm femtosecond laser light was focused to a small cross-section above the surface (~100 μm diameter), and very high intensities in the 10^{14} W cm^{-2} regime have been realized. In both postionization methods, the laser light was introduced as close as possible to the surface in order to minimize the negative effect of particle dispersion and to achieve a good overlap of the secondary particle cloud with the ionization laser. However, the proximity to the surface is limited by the possible ablation of the sample by outer portions of the ionization laser beam. We estimate that the distance of the ionization laser to the target surface was ~0.2–0.5 mm.

RESULTS AND DISCUSSION

To obtain a reference for the removal rates of LD, all samples (Al, Cu, Zr, In and Au) were analyzed by Ar^+ ion sputtering and N_2 LD. For each atomization method, postionization with the ArF excimer laser and the femtosecond laser were performed in a single, two-channel experiment by alternating between the two postionization lasers. Fluctuations in the rate of material removal can be averaged out by interleaving the measurements in this fashion. Thus, we can assume that the signal in both channels represents the same number of removed atoms. The mass spectra shown in this paper are normally the sum of 100–1000 individual shots, depending upon the signal levels and/or the relative removal rates. In a similar procedure, we have also recorded the signals of directly emitted ions and postionized atoms by interleaving measurements. In this case, the ionization laser was not triggered every other removal cycle. In this manner, the contribution of direct ions in the postionization spectra can easily be determined.

Useful yield of the apparatus

The useful yield of a surface analysis device is defined as the ratio of detected atoms to removed atoms. This ratio will depend on the removal conditions and the postionization method. A high useful yield is especially important if an analysis with minimum surface damage and/or very little sample consumption is desired.

For this determination Ar^+ ion-sputtered Al and postionization with 193 nm laser radiation were chosen for two reasons. First of all, the number of removed atoms can be calculated in a straightforward fashion and, secondly, photoionization of Al atoms can be achieved with a single 193 nm photon due to the low ionization potential of 5.986 eV and fortuitous autoionization resonances.[28]

The ionization efficiency can be defined as the ratio of photoionized atoms to removed secondary atoms. High ionization efficiency requires a high-ionization cross-section, as well as good overlap of the desorbing particle cloud with the ionizing laser. For this reason, the ArF laser was intentionally defocused in front of the sample to enlarge the ionization volume (~4 mm^2 cross-section). Despite the lower laser intensity, saturation of the Al photoion signal was still established.

Using the sputter yield for polycrystalline Al ($Y = 2.8$)[29] and the detector signal produced by an individual ion on the microchannel plate detector, the ratio of detected atoms to removed atoms was determined for Al. This useful yield includes ionization efficiency and transmission of our ToF instrument. Measurements on a pure Al sample have shown undesirable space-charge effects. Unfortunately, decreasing the length of the primary ion pulse is not a good solution to this problem

due to instabilities created in the primary ion pulse. In order to avoid the space-charge effects, the useful yield has been determined using a NIST glass standard with an Al concentration of 10 181 ppm. Assuming a sputter yield of $Y = 1$ for this glass target, we found a useful yield for ion-sputtered Al and 193 nm postionization of ~2%.

Comparison of femtosecond laser and ArF laser postionization

The comparison between ArF laser postionization and femtosecond laser postionization was performed in a single experiment by alternating the ArF and femtosecond laser ionization and averaging over 100–1000 individual shots. Fluctuations in the desorption yield from shot to shot are negligible in such an experiment and both channels represent with high accuracy the same number of removed atoms. The ratio of the signal levels is therefore equal to the ratio of the useful yields for the two ionization lasers.

The parameters that determine the number of ionized atoms for a certain species and removal technique are the wavelength, the laser intensity, the pulse length and the number of secondary neutrals in the ionization volume during the laser pulse. The laser wavelengths, 193 nm and 248 nm, are non-resonant for all analyzed materials in this study (excluding Al with 193 nm). Photoionization with 193 nm laser radiation is a one-photon process for Al and In, while ionization of Cu, Zr and Au requires a two-photon process. Photoionization with 248 nm laser radiation is a two-photon process for all elements in the present study, as it is with most elements.

The pulse length of both ionization lasers is short enough to ensure that an insignificant number of atoms enters or leaves the ionization volume during this time period, and the photoion signal is proportional to the number of atoms in the ionization volume. As a result, the ionization efficiency depends on the size of the ionization volume and the number density of secondary neutrals. A high particle density can be established when the secondary neutrals originate from a small surface area and when the postionizing laser beam is near the surface. The femtosecond laser ionization was performed with a well-focused beam in front of the target that resulted in a rather small ionization volume. To compensate, the irradiance was applied very close to the surface with very high intensities. In contrast, the ArF laser ionization was accomplished with a large ionization volume and intensities almost seven orders of magnitudes lower. Ion sputtering followed by femtosecond laser postionization cannot be very efficient under our experimental conditions. Only a very small part of the secondary particle cloud can overlap with the ionization volume due to the small ionization volume compared to a large primary ion beam. For this reason, the measurements for all samples show higher signal levels for the combination 'ion sputtering + ArF laser' compared to 'ion sputtering + femtosecond laser.'

Correspondingly, in the following discussion we will concentrate on measurements with LD. In the desorption regime, the main fraction of the desorbed species are emitted as neutrals. Operating in this regime requires that the intensity of the N_2 laser be attenuated to avoid a plasma plume along with the undesired emission of a large number of direct ions. To achieve a high desorption yield for neutral atoms, the ablation laser power was kept just below the threshold for plasma formation. The neutrals originate from a comparably small surface area, typically in the range 1 μm^2; the spot size was determined simply by observing the crater formation on the target using the Schwarzschild microscope.

In Fig. 4, mass spectra of laser-desorbed Au atoms with femtosecond laser and ArF laser postionization are shown. The intense femtosecond laser radiation is capable of double and even triple ionization of the desorbed Au atoms. The ionization potential (IP) of 20.5 eV for Au II already requires a non-resonant, five-photon process for 248 nm radiation. Unfortunately, no value for the IP of Au III has been found in the literature. Figure 4 shows also a signal comparison between ArF laser ionization and femtosecond laser ionization; it can be concluded that the useful yield for femtosecond laser ionization is considerably higher than for ArF laser ionization.

Figure 5 shows a mass spectrum for laser-desorbed In with femtosecond laser postionization; the enlarged part of the spectrum shows traces of iron that originate from depositions due to previous sputtering of the stainless-steel target holder. Iron has been found to some extent in all spectra with femtosecond laser postionization, since iron can be easily ionized due to a resonant excitation with 248 nm radiation. The In^{2+} signal has been found to be even higher than the In^+ signal. However, the first ionization of In is more efficient for ArF laser radiation since the low IP of 5.786 eV requires only a one-photon process for 193 nm radiation and saturation is easily achieved.

The results for laser ablation with femtosecond postionization of Cu and Zr are similar and also show a considerable number of doubly ionized atoms. The signal ratio of Cu^{2+}/Cu^+ varies between 10 and 30%

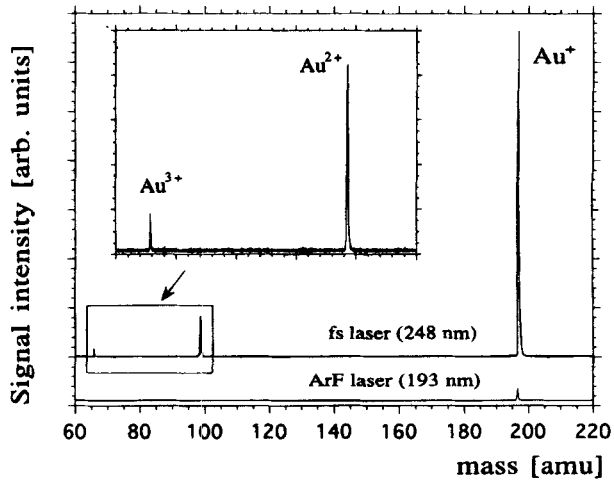

Figure 4. Time-of-flight mass spectra of laser-desorbed Au atoms. Postionization was accomplished with femtosecond laser and ArF excimer laser radiation in a single experiment by alternating between the two lasers using two-channel data acquisition. The intense femtosecond laser radiation of 10^{14} W cm^{-2} is capable of double and even triple ionization of the desorbed Au atoms. The comparison of the two postionization methods shows much higher signal levels for the femtosecond laser.

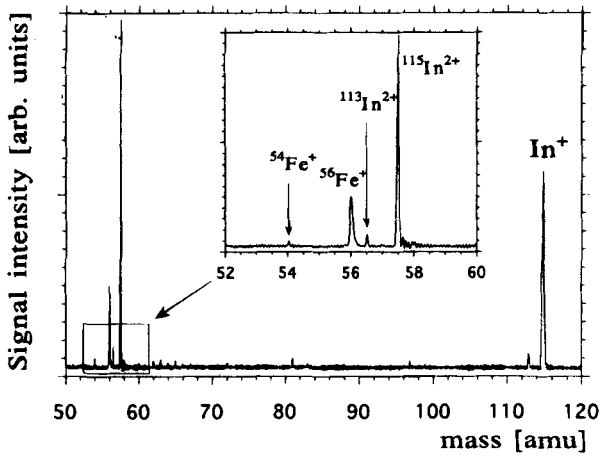

Figure 5. Time-of-flight mass spectra for laser-desorbed In and femtosecond laser postionization. The In^{2+} signal is even higher than the In^{+} signal. The enlarged part of the spectrum shows traces of iron which were deposited during previous sputtering of the sample holder.

for different measurements, with the ionization efficiency roughly a factor of five better than in the ArF laser ionization. The femtosecond laser postionization of laser-desorbed Zr has revealed approximately equal numbers of singly and doubly charged atoms, but triply charged Zr ions have also been observed.

Fluctuations in the fraction of multiply charged species are inherent in the different measurements, since the very high intensities of the femtosecond radiation cannot be reproduced with high precision. Furthermore, the intensity profile of the femtosecond laser is less homogenous than the intensity profile of the ArF laser; the well-focused femtosecond laser beam with its small spot size is certainly less homogenous than the ArF laser beam. A perfect ionization volume would require a uniform intensity profile over a well-defined cross-section; an inability to assure this is a problem inherent in all postionization techniques. Appearance of multiply charged ions is an indicator of ionization saturation nominally in parts of the ionization volume. However, a quantitative analysis with NRMPI requires that the saturation volume size does not vary among different species.

The applied femtosecond laser radiation approaches an intensity regime where electric field ionization from the electronic ground state may occur. Such a tunneling ionization (TI) mechanism can be understood in terms of a Coulomb barrier suppression due to the laser radiation field.[30] This TI or ponderomotive regime can be distinguished from the NRMPI regime by introducing the Keldysh parameter $\gamma = (IP/2\Phi)^{1/2}$, where IP stands for the ionization potential of an atom or ion and Φ for the ponderomotive potential. This ponderomotive potential is the average kinetic energy of an oscillating electron in the laser radiation field; it is proportional to the laser intensity and the square of the laser wavelength.[31] Ponderomotive ionization corresponds to $\gamma < 1$, whereas $\gamma > 1$ indicates the NRMPI regime. Our experimental parameters are in accordance with $\gamma \sim 2$–3 for single ionization and $\gamma \sim 3$–4 for double ionization at the highest intensity levels (10^{14} W cm^{-2}). Lower laser intensities yield $\gamma \gg 1$, and we conclude that femtosecond laser ionization is governed by multi-photon processes in these experiments. Recent experiments with similar laser intensities but at a laser wavelength of 800 nm have shown evidence for concurrent ionization by NRMPI and TI.[7]

Comparison of ion sputtering and LD

To estimate the rates of removal by the N_2 ablation laser, we have compared signal levels of measurements with ion sputtering and LD. For this comparison, we chose the ArF laser ionization for two reasons: only the ArF laser can ensure good overlap with the secondary particle cloud in both removal methods; and better reproducibility of the laser intensity.

As already mentioned, the LD experiments were performed with intensities just below the threshold for plasma formation. The ToF mass spectra of laser-desorbed species with and without postionization show that the amount of direct ionization is insignificant in this desorption mode; >90% of the secondary particles are neutral atoms.

For all five elements, the signal levels for LD + ArF laser ionization are comparable to the signal levels for 'ion sputtering + ArF laser ionization'. In Fig. 6 such a comparison is shown for postionized Cu and Zr atoms. However, the photoion signal cannot be directly related to the number of removed atoms. The useful yields of the two removal methods, ion sputtering of LD, differ for several reasons.

First of all, the emission process is much shorter in time for LD compared to ion-sputtering due to a 800 ns primary ion pulse. In principle, the generation of much shorter ion pulses is possible, but only at the expense of primary ion current on the target. In the LD mode the particles are emitted within a few ns. For metal surfaces a thermal desorption mechanism is expected. In this case, the desorption rate correlates with the vapor pressure, which means an exponential dependence on the surface temperature. Theoretical calculations of surface heating during laser irradiation suggest that the particle emission is only slightly longer than the primary laser pulse.[32] The emission velocities of thermally desorbed

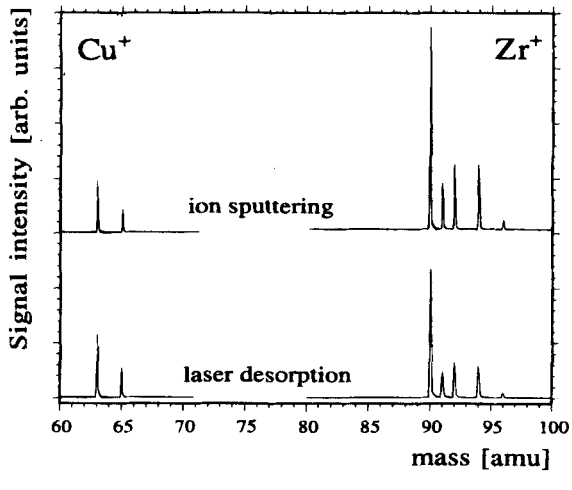

Figure 6. Time-of-flight mass spectra for Cu and Zr with ArF laser ionization. The comparison between laser desorbed and ion-sputtered atoms reveals similar signal levels.

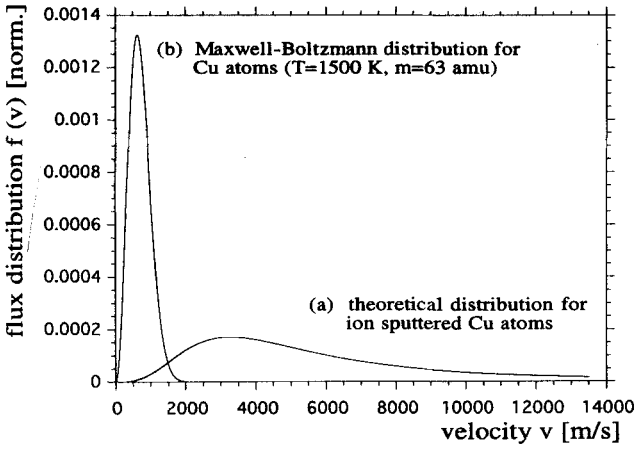

Figure 7. Comparison of laser desorbed and ion-sputtered atoms. Curve (a) shows the expected velocity distribution for ion-sputtered Cu atoms. Curve (b) corresponds to a Maxwell–Boltzmann distribution with $T = 1500$ K, which is a realistic temperature for laser-induced thermal desorption of Cu.

particles can be approximated by a Maxwell–Boltzmann distribution; for laser-desorbed atoms temperatures of typically <2000 K have been found.[33]

Since the desorption process is short compared to the flight time of secondary neutrals, a simple estimate of particle emission velocities can be made. We assume a time delay between the desorption laser pulse and the ionization laser pulse of Δt, a distance d between the surface and ionization volume and a length s of ionization volume (in the direction of the ToF-MS axis). Following this, the ionization process selects a certain fraction of the velocity distribution of the desorbed neutrals whereby only secondary neutrals with velocities between $d/\Delta t$ and $(s + d)/\Delta t$ can be ionized.

At this point, it should be mentioned that the velocity distribution of the laser-desorbed atoms deviates significantly from ion-sputtered atoms. The emission of ion-sputtered atoms in our experiments is governed by elastic collision in the solid. Therefore, the emission process of the ion-sputtered species can be described quite well by a collisional cascade model[14] where the surface binding energy of the sample is the relevant parameter. The energy distribution of ion-sputtered particles peaks typically at energies of ~ 1 eV.[11,34]

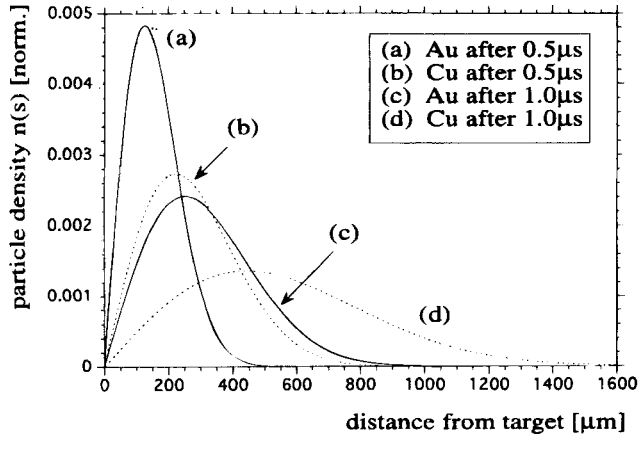

Figure 8. Particle density distribution of Cu (dashed lines) and Au (solid lines) atoms as a function of the distance from the target surface. The dispersion of the secondary particle cloud is shown 0.5 μs and 1.0 μs after the desorption. A Maxwell–Boltzmann distribution with $T = 1500$ K has been assumed for Cu and Au atoms, respectively.

Figure 7 shows a comparison of velocity distributions which can be expected from LD and ion sputtering. Curve (a) is the expected distribution for ion-sputtered Cu atoms; it is based on an energy distribution $f(E) \propto E/(E + U_b)^3$ with a surface binding energy $U_b = 3.5$ eV. This Thompson distribution[1] has been found to be in excellent agreement with experimental results found for sputtered atoms.[10] Curve (b) corresponds to a Maxwell–Boltzmann distribution for Cu atoms with $T = 1500$ K, which is a realistic temperature for laser-induced thermal desorption of Cu. As shown, thermally desorbed atoms are in general much slower than ion-sputtered atoms, and more importantly they have a much narrower velocity distribution. For ion sputtering, we found that an 800 ns primary ion pulse length is necessary to maximize the SNMS signal. This is a consequence of the broad velocity distribution of sputtered atoms and results in a limitation of the achievable useful yield.

Based on a Maxwell–Boltzmann distribution for $T = 1500$ K, we calculated the particle density distribution for Cu and Au atoms. Figure 8 shows the density distributions 0.5 μs and 1 μs after the desorption pulse as a function of the distance from the target. The angular distribution of the secondary particles has not been taken into account; this would result in a broader distribution with a peak shift towards the target surface, but it would not change the following conclusions drawn from Fig. 8.

For a small ionization volume (defined by the laser beam cross-section) the best useful yields are achieved if the ionization laser is as close as possible to the sample surface and triggered shortly after the desorption pulse. It is also evident that mass fractionation might occur depending on the size of the ionization volume and the distance from the target to the ionization laser. For example, LD of a multicomponent sample (e.g. an alloy) will result in the emission of secondary particles with the same temperature. Nevertheless, due to different masses, the desorbed atoms will disperse differently in time, as shown for Cu and Au atoms in Fig. 8.

The degree of mass fractionation will depend primarily on the size of the ionization volume, on the position of the laser beam relative to the ablated surface area and the time delay between desorption and postionization. On the other hand, LD has the advantage that very high useful yields can be established for a particular mass. It is evident from Fig. 8 that a laser beam >1 mm in diameter can ionize most of the desorbed atoms if saturation is achieved and mass fractionation can be minimized over a wide mass range. Regarding the measurements performed on Al with ArF laser postionization, we estimate for LD a useful yield of $>10\%$, which means at least an improvement by a factor of five compared to the 2% value found for ion sputtering.

SUMMARY AND OUTLOOK

Laser desorption of neutral atoms coupled with laser postionization has been found to be an excellent combination for ToF-MS. The removal process from a very

small surface area and efficient postionization (e.g. by intense femtosecond laser radiation) guarantee little sample consumption and a high useful yield for our laser microprobe instrument.

The observation of multiply charged ions with femtosecond laser ionization indicates saturation in the ionization volume. Saturation of the photoionization signal for all secondary particles in a multicomponent sample allows an easy calculation of the concentration of each species in the sample as long as molecular fragmentation does not play an important role. However, the saturation volume size certainly varied among the elements in this study since the ratios of multiply charged to singly charged ions differed.

One major problem of laser ablation is certainly the reproducibility of the desorption yield due to the highly non-linear dependence of the particle yield on the laser intensity; small fluctuations of the energy density at the surface may lead to large fluctuations in the desorption yield. As a result, the stability of the ablation laser output, the surface topography, the reflectivity and the surface make-up will play important roles in the reproducibility of the desorption yield.

The high spatial resolution of laser microprobe analysis could be used for mapping the elemental composition of the surface. A remote-controlled scan of the sample in the x–y direction and synchronization with the desorption and ionization lasers would enable imaging over a limited surface area. An important feature of mapping with this technique is that an entire mass spectrum is collected at each x–y point.

Acknowledgements

This work was supported by the US Department of Energy, BES-Materials Sciences, under Contract W-31-109-ENG-38 and by National Aeronautics and Space Administration through grants NAGW-3345 (to Robert N. Clayton, University of Chicago) and NAGW-3384 (to A.M.D.). D. E. M.'s work was performed at Argonne National Laboratory while a Faculty Research Participant (program administered by the Argonne Division of Educational Programs with funding provided by the US Department of Energy).

REFERENCES

1. R. Behrisch and K. Wittmaack (eds), *Sputtering by Particle Bombardment III*, Vol. 64. Springer-Verlag, Berlin (1991).
2. H. Gnaser and W. O. Hofer, *Appl. Phys. A* **48**, 261 (1989).
3. W. Gerhard and H. Oechsner, *Z. Phys. B* **22**, 41 (1975).
4. C. E. Young, W. F. Calaway, M. J. Pellin and D. M. Gruen, *J. Vac. Sci. Technol. A* **2**, 693 (1984).
5. C. H. Becker and K. T. Gillen, *Appl. Phys. Lett.* **45**, 1063 (1984).
6. C. H. Becker and K. T. Gillen, *Anal. Chem.* **56**, 1671 (1984).
7. M. L. Wise, A. B. Emerson and S. W. Downey, *Anal. Chem.* **67**, 4033 (1995).
8. C. H. Becker and J. S. Hovis, *J. Vac. Sci. Technol. A* **12**, 2352 (1994).
9. M. J. Dryer, L. E. Jusinski, H. Helm and C. H. Becker, *Appl. Surf. Sci.* **52**, 151 (1991).
10. S. R. Coon, W. F. Calaway, J. W. Burnett, M. J. Pellin, D. M. Gruen, D. R. Spiegel and J. M. White, *Surf. Sci.* **259**, 275 (1991).
11. A. Wucher, M. Wahl and H. Oechsner, *Nucl. Instrum. Methods B* **82**, 337 (1993).
12. N. Winograd, J. P. Baxter and F. M. Kimock, *Chem. Phys. Lett.* **88**, 581 (1982).
13. N. S. Nogar and R. C. Estler, *Anal. Chem.* **57**, 2441 (1985).
14. P. Sigmund, *Phys. Rev.* **184**, 383 (1969).
15. L. Van Vaeck, H. Struyf, W. Van Roy and F. Adams, *Mass Spectrom. Rev.* **13**, 189 (1994).
16. U. Boesl, R. Weinkauf, C. Weickhardt and E. W. Schlag, *Int. J. Mass. Spectrom. Ion Process.* **131**, 87 (1994).
17. E. H. Piepmeier, in *Analytical Applications of Lasers*, ed. by E. H. Piepmeier, pp. 627–669. Wiley, New York (1986).
18. A. J. Peurrung, J. P. Cowin, G. Teeter, S. E. Barlow and T. M. Orlando, *J. Appl. Phys.* **78**, 1 (1995).
19. C. R. Ayre, L. Moro and C. H. Becker, *Anal. Chem.* **66**, 1610 (1994).
20. Z. Ma, R. N. Thompson, K. R. Lykke, M. J. Pellin and A. M. Davis, *Rev. Sci. Instrum.* **66**, 3168 (1995).
21. K. Schwarzschild, *Astron. Mitt. Sternwarte* **10**, 3 (1905).
22. P. Erdös, *J. Opt. Soc. Am.* **49**, 877 (1959).
23. M. T. Asaki, C.-P. Huang, D. Garvey, J. Zhou, H. C. Kapteyn and M. M. Murnane, *Opt Lett.* **18**, 977 (1993).
24. J. Squier, F. Salin, G. Mourou and D. Harter, *Opt. Lett.* **16**, 324 (1991).
25. I. N. Ross, A. R. Damerell, E. J. Divall, J. Evans, G. J. Hirst, C. J. Hooker, J. R. Houliston, M. H. Key, J. M. D. Lister, K. Osvay and M. J. Shaw, *Opt. Commun.* **109**, 288 (1994).
26. A. P. Schwarzenbach, T. S. Luk, I. A. McIntyre, U. Johann, A. McPherson, K. Boyer and C. K. Rhodes, *Opt. Lett.* **11**, 499 (1986).
27. S. Szatmari, F. P. Schafer, E. Muller-Horsche and W. Muckenheim, *Opt. Commun.* **63**, 305 (1987).
28. R. L. Kelly, *Atomic and Ionic Spectrum Lines Below 2000* Å (*H through Ar*). Controlled Fusion Atomic Data Center, Oak Ridge National Laboratory, USA (1982).
29. N. Matsunami, Y. Yamamura, Y. Itikawa, N. Itoh, Y. Kazumata, S. Miyagawa, K. Morita, R. Shimizu and H. Tawara, *At. Data Nucl. Data Tables* **31**, 1 (1984).
30. S. Augst, D. D. Meyerhofer, D. Strickland and S. L. Chin, *J. Opt. Soc. Am. B* **8**, 858 (1991).
31. L. V. Keldysh, *Sov. Phys. JETP* **20**, 1307 (1965).
32. P. Wurz and K. R. Lykke, *Chem. Phys.* **176**, 185 (1993).
33. P. Wurz, K. R. Lykke, M. J. Pellin and D. M. Gruen, *J. Appl. Phys.* **70**, 6647 (1991).
34. S. R. Coon, W. F. Calaway, M. J. Pellin, G. A. Curlee and J. M. White, *Nucl. Instrum. Methods Phys. Res. B* **82**, 329 (1993).